Incorporating Human Visual Model and Spatial Sampling in Banding Artifact Reduction

Cheng-Lun Chen and George T.-C. Chiu, *Member,ASME and IEEE*

Abstract— **Halftone banding, which affects the uniformity of xerographic images, is a well-known artifact for xerography, which appears as periodic light and dark bands across a printed page perpendicular to the process or print direction. Effective approaches for banding compensation need to consider the following two unique characteristics: 1) The human visual system should be included into the control system synthesis to quantify the perceived banding; 2) Spatially periodic scanline spacing variation due to gear noise has been shown to be a major contributor. In this paper, we will summarize the work to incorporated human visual model into control system design and point out one aspect of the human visual system model that will need to be addressed. To handle position dependent periodic disturbances, we will employ spatial sampling and reformulate the motion transmission system using angular displacement as the independent variable. A linear parameter varying repetitive controller (LPVRC) is proposed to compensate for the angular displacement dependent periodic disturbances caused by the gears. Experimental verifications of the proposed approach will be presented.**

I. Introduction

HALFTONE banding, which affects the uniformity of xerographic images, is a well-known artifact which appears as periodic light and dark bands across a printed page perpendicular to the process or print direction. Among the causes of banding, scanline spacing variation is a major contributor. It is known that scanline spacing variation should be within 1% of the process resolution to avoid noticeable artifact [1]. For a moderate 1200 dpi printer capable of printing at 36 pages per minute, a positioning accuracy of 0.2 μm at a linear speed of 167 mm/sec is needed. Ideally, the photoreceptor speed is designed to be constant to maintain uniform scanline spacing. However, even with sophisticated control, transmission error, load variation, and manufacturing tolerance will still have significant impact on the final scanline spacing. Periodic nature of banding usually points its source towards gear transmission errors, e.g., eccentricity and tooth profile error. This indicates the importance of designing and controlling the motion systems in the xerographic, also known as the electrophotographic (EP) process.

This work was supported in part by the National Science Foundation under Award CMS-0201837

Cheng-Lun Chen was with the School of Mechanical Engineering, Purdue University. He is now with the Lexmark International, Lexington, KY 40517 (e-mail: chenglun02@hotmail.com).

George T.-C. Chiu is with the School of Mechanical Engineering, Purdue University, West Lafayette, IN 47907 USA, (Phone: 765-494-2688, e-mail: gchiu@purdue.edu).

Many studies have been reported on reducing banding in EP processes. These studies can be categorized into the following four approaches: 1) To design better transmission, i.e., gear meshing or gear pitch, to either reduce transmission error or move the vibration into higher frequency region where human visual system is less sensitive [2-4]; 2) To deflect the laser beam in the print or process direction to compensate for the line spacing variation [5-8], 3) To modulate the laser power to directly compensate for the absorptance variation due to scanline spacing error [9-13]; 4) Using halftone techniques to mask banding artifacts [14-16]. Recently, studies have soon that well designed closed-loop regulation of the photoreceptor drum velocity can be effective in reducing the perceivable banding [17]. An advantage of using feedback control is its ability to reduce system sensitivity to uncertainties (such as consumable change and component aging). However, since banding involves spatially periodic disturbances, temporal based controller design is complicated with frequency variation due to fluctuation in nominal velocity. In this paper we will discuss an approach to formulate the control problem in the angular displacement domain so that the fluctuation in the nominal velocity will be taken into consideration in the problem formulation, which results in a more robust design.

Image quality is one of the more important metrics that impacts the performance and competitiveness of an image rendering system. An overall image quality metric should depend on the combination of all the above-mentioned attributes. Image quality is a subjective experience. Therefore, a valid image quality metric should not neglect the role of human perception. A reasonable image quality metric should incorporate human perceptual mechanism into its computation algorithm to correlate objective measurement with perception.

Due to the periodic nature of banding, Fourier analysis has been widely used to characterize banding. One issue with using Fourier analysis alone to quantify banding lies in the fact that for sinusoidal or periodic reflectance fluctuation, human eyes are less sensitive to extremely low and very high frequency reflectance variation. Thus, a model of the human visual system (HVS) is needed to reflect the actual perceived banding. The contrast sensitivity function (CSF) is a model that uses the modulation transfer function (MTF) to characterize of the HVS in perceiving spatially periodic contrast variations. Several researches have contributed to the analysis and synthesis of the CSF function [18-20], see Fig. 1.

Note that the bandpass-like CSF function implies that mid-frequency disturbances have greater impact on perceived banding. A banding reduction scheme should employ more effort to reduce bandings in this frequency region.

Since actual banding artifact consists of more than one frequency components. The perceived visual impact for multi-frequency stimuli is important. There is suggestion [21] that perceptual response to mixed frequency luminance variation would be simply the linear summation of the perceptual response to each individual frequency. However, this is not true when there are reflectance fluctuations with frequency values close to one another that cause frequency beat. The example shown in Fig. 2 demonstrates beat phenomenon for a stimuli with two frequency components. This example also points out the insufficiency of the CSF weighted FFT on reflectance measurement approach. The human visual system model for banding assessment needs to be revisited.

One popular HSV model for assessing perceived periodic stimuli is proposed in [22]. Based on this model, the first stage of the visual system is composed of a linear transduction phase that provides signals for a set of spatial frequency tuned channels. These channels operate in parallel and carry independent information to a decision process. Though the range of spatial frequencies processed by a given channel is unclear, the largest estimates are approximately two octaves. This model also implies that there are three stages in the human visual system to process spatial information. One of these stages is a FFT-like filtering of the preprocessed signals done by the sensory stage. This somewhat supports the methodology of characterizing periodic banding for an image by performing Fourier analysis on the image signals. Many researchers have been using strategies combining FFT and CSF to evaluate image quality.

The occurrence of spatial beat in visual systems has been documented since 1973 [23]. Spatial beat is a variation in contrast that is periodic but has no power in the spatial frequency domain at the beat frequency. Logvinenko's experiments[24] supported the hypothesis that beat is caused by distortion product in the sensory stage. A nonlinear cascade human visual model, as shown in Fig. 3, was proposed and verified by experimental data. Logvinenko attempted to explain the neurological basis of his 3-stage model. The first stage of the model can be viewed as a high bandwidth filter and the third stage as a CSF-like bandpass filter. Both are linear. Note also that the proposed hyperbolic function in the middle stage can be approximated by a logarithmic function. This model is attractive since it can predict the beat frequency by cascading a nonlinear operator with a CSF-like linear filter. In this paper, we will also propose methods to incorporate this type of performance metric into the controller design method.

The remaining of the paper is organized as follows. The cascade HVS model for contrast variation will be discuss in the next section. The proposed angular displacement formulation of the velocity regulation control will be discussed in the third section followed by the discussion of experimental verifications. Conclusion will be given in the last section.

II. Human Visual Model for Banding Analysis

Before any approach is developed to reduce banding artifact, method to quantitatively measure perceived banding needs to be developed.

A banding test page is constructed that consists of some halftoned images and a percentage-filled pattern. Once the test page is printed, a high-resolution flatbed or drum scanner is used to scan in the printed test pattern. Before scanning the printed test page, the scanner needs to be calibrated. Scanner calibration is to obtain a tone or gamma correction function, $TCF(\cdot)$, using a standard calibration target. For a monochrome scanner, the tone correction curve maps the captured digital gray value to its actual gray value. That is, $R(x,y) = TCF[R_0(x,y)]$, where $R(x,y)$ represents the actual gray value and $R_0(x,y)$ represents the scanned gray value.

The tone corrected reflectance or absorptance data is then averaged row-wise in the direction perpendicular to the process direction to form a 1-D reflectance array. As mentioned in the previous section, the CSF weighted reflectance is insufficient in explaining some phenomenon (i.e., beat) due to neglecting of the nonlinear distortion within the human visual system. In this study, we will incorporate the CSF weighted FFT method and explore the feasibility of a cascaded model with a nonlinear operator preceding the FFT block, see Fig. 4. Specifically, we will be focusing on determining a nonlinear mapping to predict frequency beat.

Assuming a static nonlinearity, the nonlinear operator or distortion can be expressed as

$$y = \log(x) = \log L + \log(1+f) = \log L + f - f^2/2 + \ldots ,$$

where x is the stimulus to the sensory stage, y is the output of the frequency tuned channel and $x = L(1+f)$ where $-1 \le f \le 1$, If $f = \sin(w_1 t) + \sin(w_2 t)$, then the distortion product term (f^2) will have a term $\sin(w_1 t)\sin(w_2 t)$, which will contribute a frequency component at $(w_1 - w_2)$. Note that the use of logarithmic or power function for the nonlinear operator can be viewed as conversion from reflectance or luminance to brightness or lightness. Three types of nonlinear operations will be investigated.

Define the nonlinear mapping as NL: $R \rightarrow L$, where R is the reflectance the can be expressed as $R(y) = \bar{R} + \Delta R(y)$, where y is the pixel position along the process direction, $\bar{R}$ is the background or average reflectance and $\Delta R(y)$ is the corresponding reflectance variation.. The three nonlinear operators under consideration can be formulated as:

1. Half rectification: $L = NL(R) = \begin{cases} R, & \mathrm{R} \ge \bar{\mathrm{R}} \\ \bar{R}, & \mathrm{R} < \bar{\mathrm{R}} \end{cases}$
2. Logarithmic function:
$$L = NL(R) = \log(R) = \log(\bar{R}) + \log(1 + \Delta R/\bar{R})$$
3. CIE L^*: $\quad L = NL(R) = 116 \times \left(\frac{R}{255}\right)^{1/3} - 16$

In the following simulation study, we will investigate the

situations when there are four sinusoidal components at 80, 85 , 10, and 12 [cycles/in] in the reflectance variation. Define $B(f)$ as the output from the cascaded model shown in Fig. 4, then

$$B(f) = \left| FFT[NL[TCF(R_0(y))]](f) \right| * CSF(f) \qquad (1)$$

Mannos' CSF will be used as the weighting in Eq. (1). The test pattern can be seen in Fig. 5. The results are summarized in Fig. 6. As expected, the frequencies at 10 and 12 cycles/in will be most visible. Besides, it is interesting to notice that the two beat frequencies at 5 and 2 cycles/in can be identified on the two lower plots.

Simulation results have shown that by processing the reflectance signal through a logarithmic function or the *CIE L** conversion before taking FFT and filter through the CSF, it is possible to capture the frequency part of the visible beat phenomenon. However, it is still doubtful that the relative magnitude for each frequency component is predicted correctly. More psychophysical experiments are needed.

III. Spatial Sampling Based Closed-Loop Banding Reduction

The motor/gear transmission subsystem within a typical laser printer is shown in Fig. 7. The system consists of a main brushless dc (BLDC) or stepper motor with its onboard driver and a gear train that connects to the photoconductor (PC), in this case is an organic photoconductive (OPC) drum. The task of the main motor is to supply torque to preserve constant angular velocity of the photoconductor. The driver controls the velocity of the motor by adjusting the amount of winding currents (in BLDC motors) or the stepping rate (in stepper motors). The motor shaft drives the gear train that connects with the OPC drum. Phase locked loop (PLL) and pulse width modulation (PWM) are two of the most popular methods utilized motor drivers for achieving the desired velocity regulation.

A. Position-dependent Disturbances

Many researches have shown that velocity fluctuation of the PC is one of the main causes of banding. In a typical laser printing process, the low-pass filtering of the load inertia and high-speed operation of the main motor drive usually render the effect of motor torque ripples on the PC velocity negligible. Most of the velocity fluctuations come from gear eccentricity and tooth profile error, both are angular periodic and position-dependent. They can be further characterized by analyzing the PC velocity signals sampled at equal angular displacement interval, also known as order analysis. Order spectrum obtained from order analysis provides a direct link between a frequency and the corresponding gear component. Figure 7 shows the motor/gear transmission configuration for a typical 600-dpi monochrome laser printer. The order spectrum was obtained by taking the OPC position/velocity sampling at 2500 samples/rev. The largest peak at 384 cycles/rev corresponds to the meshing between the large gear on shaft 1 and the pinion on the motor shaft. The peak at 96 cycles/rev corresponds to the meshing between the large gear on shaft 2 and the small gear on shaft 1. The peak at 48 cycles/rev was due to the eccentricity of the motor shaft. The peak at 32 cycles/rev, which is equal to 8.65 cycles/in under the nominal speed, was caused by the OPC drum.

B. Nonlinear Position-invariant System

Suppose a state space realization of an LTI model for the motion subsystem can be expressed as

$$\begin{bmatrix} \dot{x}(t) \\ z(t) \\ y(t) \end{bmatrix} = \begin{bmatrix} A & B_v & B_u \\ C_z & D_{zv} & D_{zu} \\ C_y & D_{yv} & 0 \end{bmatrix} \begin{bmatrix} x(t) \\ v(t) \\ u(t) \end{bmatrix}, \qquad (2)$$

where $x(t)$ is the state vector, $z(t)$ is the banding metric, $y(t)$ is the measurement, $v(t)$ denotes output disturbances, and $u(t)$ is the control input. Instead of using time t as the independent variable, it is possible to consider an alternative independent variable $\phi = f(t)$, which is a strictly monotonic function of t such that its inverse $t = f^{-1}(\phi)$ exists. The time domain variables can be transformed into their counterparts in the ϕ-domain. Since

$$\frac{dx}{dt} = \frac{d\phi}{dt}\frac{d\tilde{x}}{d\phi},$$

Eq. (2) can be rewritten as

$$\begin{bmatrix} \frac{d\phi}{dt}\dot{\tilde{x}}(\phi) \\ \tilde{z}(\phi) \\ \tilde{y}(\phi) \end{bmatrix} = \begin{bmatrix} A & B_v & B_u \\ C_z & D_{zv} & D_{zu} \\ C_y & D_{yv} & 0 \end{bmatrix} \begin{bmatrix} \tilde{x}(\phi) \\ \tilde{v}(\phi) \\ \tilde{u}(\phi) \end{bmatrix}. \qquad (3)$$

Let $\theta(t)$ be the angular displacement of the OPC in the motion system. Let $\phi = \theta(t)$, then since $\theta(t) = \int_0^t w(\tau)d\tau,$, where $w(t)$ is the angular velocity, the following condition

$$w(t) = \frac{d\theta}{dt} > 0, \ \forall \ t > 0$$

will guarantee that $\theta(t)$ is strictly monotonic. In practice, this condition can be easily satisfied for a laser printing system since the imaging component such as the photosensitive drum always rotates in one direction during printing. Suppose the angular velocity is measurable by

$$\tilde{w}(\theta) = C_w \tilde{x}(\theta) + w_0 \neq 0, \qquad (4)$$

where w_0 is the nominal velocity. Substituting Eq. (4) into Eq. (3) and imposing the saturation function $sat(.)$ on $\tilde{u}(\theta)$, we obtain

$$\begin{bmatrix} \dot{\tilde{x}}(\theta) \\ \tilde{z}(\theta) \\ \tilde{y}(\theta) \end{bmatrix} = \begin{bmatrix} A/(C_w\tilde{x} + w_0) & B_v/(C_w\tilde{x} + w_0) & B_u/(C_w\tilde{x} + w_0) \\ C_z & D_{zv} & D_{zu} \\ C_y & D_{yv} & 0 \end{bmatrix} \begin{bmatrix} \tilde{x}(\theta) \\ \tilde{v}(\theta) \\ sat(\tilde{u}(\theta)) \end{bmatrix}. \qquad (5)$$

The system expressed by the equation above is a nonlinear position-invariant system with the angular position θ as the independent variable.

C. LPV Gain-scheduling Design

The OPC drum angular velocity, i.e., Eq. (4), is measurable in real-time. In addition, the input and output of the actuator saturation model can also be monitored online if the saturation model is known. By defining two varying parameters

$$\rho = \frac{1}{\tilde{w}} \text{ and } \phi = \frac{sat(\tilde{u})}{\tilde{u}},$$

we can rewrite Eq. (5) as

$$\begin{bmatrix}\dot{\tilde{x}}(\theta)\\ \tilde{z}(\theta)\\ \tilde{y}(\theta)\end{bmatrix}=\begin{bmatrix}\tilde{A}(\rho) & \tilde{B}_v(\rho) & \tilde{B}_u(\rho,\phi)\\ C_z & D_{zv} & \tilde{D}_{zu}(\phi)\\ C_y & D_{yv} & 0\end{bmatrix}\begin{bmatrix}\tilde{x}(\theta)\\ \tilde{v}(\theta)\\ \tilde{u}(\theta)\end{bmatrix}, \quad (6)$$

where

$$\tilde{A}(\rho)=A\rho,\ \tilde{B}_v(\rho)=B_v\rho,\ \tilde{B}_u(\rho,\phi)=B_u\rho\phi,\ \tilde{D}_{zu}(\phi)=D_{zu}\phi.$$

Equation (6) represents a linear parameter-varying (LPV) system with two varying parameters that can be measured in real-time. This is also a quasi-LPV system since one of the varying parameters (ρ) actually depends on the states of the system. Defining another varying parameter $\eta = \rho\phi$, such that

$$\hat{B}_u(\eta)=B_u\rho\phi,$$

we arrive at an affine LPV or polytopic system with three varying parameters, i.e.,

$$\begin{bmatrix}\dot{\tilde{x}}(\theta)\\ \tilde{z}(\theta)\\ \tilde{y}(\theta)\end{bmatrix}=\begin{bmatrix}\tilde{A}(\rho) & \tilde{B}_v(\rho) & \tilde{B}_u(\eta)\\ C_z & D_{zv} & \tilde{D}_{zu}(\phi)\\ C_y & D_{yv} & 0\end{bmatrix}\begin{bmatrix}\tilde{x}(\theta)\\ \tilde{v}(\theta)\\ \tilde{u}(\theta)\end{bmatrix}. \quad (7)$$

The controller synthesis problem for the affine LPV system is to find a parameter-dependent output feedback dynamic controller

$$\begin{bmatrix}\dot{\tilde{x}}_K(\theta)\\ \tilde{u}(\theta)\end{bmatrix}=\begin{bmatrix}\tilde{A}_K(\psi) & \tilde{B}_K(\psi)\\ \tilde{C}_K(\psi) & \tilde{D}_K(\psi)\end{bmatrix}\begin{bmatrix}\tilde{x}_K\\ \tilde{y}\end{bmatrix}, \quad (8)$$

where $\psi = (\rho, \phi, \eta)$. The solution can be obtained by solving a set of well defined LMIs, which is well documented in the literature.

D. LPV Repetitive Control (LPVRC)

To address the position dependent disturbances and control input saturation, a proposed control structure is shown in Fig. 8. Here the open-loop LPV system $G(\rho)$ can be expressed as

$$\begin{bmatrix}\dot{\tilde{x}}(\theta)\\ \tilde{q}(\theta)\\ \tilde{z}(\theta)\\ \tilde{y}(\theta)\end{bmatrix}=\begin{bmatrix}\tilde{A}(\rho) & \tilde{B}_p(\rho) & \tilde{B}_v(\rho) & \tilde{B}_u(\eta)\\ C_q & D_{qp} & D_{qv} & \tilde{D}_{qu}(\phi)\\ C_z & D_{zv} & D_{zv} & \tilde{D}_{zu}(\phi)\\ C_y & D_{yp} & D_{yv} & 0\end{bmatrix}\begin{bmatrix}\tilde{x}(\theta)\\ \tilde{p}(\theta)\\ \tilde{v}(\theta)\\ \tilde{u}(\theta)\end{bmatrix},$$

which differs slightly from Eq. (7). Here we also consider unstructured modeling uncertainty for the updated open-loop LPV system. Thus there are basically two types of perturbation affecting the open-loop system. One is due to the varying parameters, which is bounded and measurable in real-time. The other is due to modeling error, which is bounded but not measurable in real-time.

In this study, we will consider a low-order and attenuated repetitive controller, which takes the form of

$$RC(s)=\frac{1}{s/\omega_r+1}\prod_{i=1}^{k}\frac{s^2+2\zeta_i\omega_{ni}s+\omega_{ni}^2}{s^2+2\xi_i\omega_{ni}s+\omega_{ni}^2},$$

where k is the number of periodic frequencies to be rejected, ω_{ni} is the i^{th} disturbance frequency in rad/rev, and ξ_i and ζ_i are two damping ratios that satisfy $0 < \xi_i < \zeta_I < 1$. We can adjust the gain of $RC(s)$ at those periodic frequencies by varying the values of ξ_i and ζ_i. A low-pass filter of roll-off frequency ω_r is included, which serves the similar purpose as the q-filter used in a digital repetitive controller. Suppose $RC(s)$ has the following state space realization

$$\begin{aligned}\dot{\tilde{x}}_{rc}&=A_{rc}\tilde{x}_{rc}+B_{rc}\tilde{y},\\ \tilde{y}_2&=C_{rc}\tilde{x}_{rc}.\end{aligned},$$

the repetitive controller is augmented to the 'to-be-designed' LPV controller. Note that we still consider a TDOF structure for the LPV controller. Thus the controller now has three inputs $(\tilde{y}, \tilde{y}_1, \tilde{y}_2)$ and two outputs $(\tilde{u}_1, \tilde{u}_2)$.

The spatial-domain open-loop LPV system with repetitive control can be shown to have the following state-space representation

$$\left[\begin{array}{c}\dot{\tilde{x}}(\theta)\\ \dot{\tilde{x}}_{rc}(\theta)\\ \tilde{q}(\theta)\\ \tilde{z}(\theta)\\ \tilde{y}(\theta)\\ \tilde{y}_1(\theta)\\ \tilde{y}_2(\theta)\end{array}\right]=\left[\begin{array}{cc|ccccc}\tilde{A}(\rho) & 0 & \tilde{B}_p(\rho) & \tilde{B}_v(\rho) & \tilde{B}_u(\eta) & \tilde{B}_u(\eta)\\ B_{rc}C_y & A_{rc} & B_{rc}D_{qp} & B_{rc}D_{yv} & 0 & 0\\ \hline C_q & 0 & D_{qp} & D_{qv} & \tilde{D}_{qu}(\phi) & \tilde{D}_{qu}(\phi)\\ C_z & 0 & D_{zp} & D_{zv} & \tilde{D}_{zu}(\phi) & \tilde{D}_{zu}(\phi)\\ C_y & 0 & D_{yp} & D_{yv} & 0 & 0\\ 0 & 0 & 0 & 0 & \phi-1 & \phi-1\\ 0 & C_{rc} & 0 & 0 & 0 & 0\end{array}\right]\left[\begin{array}{c}\tilde{x}(\theta)\\ \tilde{x}_{rc}(\theta)\\ \tilde{p}(\theta)\\ \tilde{v}(\theta)\\ \tilde{u}_1(\theta)\\ \tilde{u}_2(\theta)\end{array}\right]. \quad (9)$$

Making the following definitions

$$\tilde{X}=\begin{bmatrix}\tilde{x}\\ \tilde{x}_{rc}\end{bmatrix},\ \tilde{Z}=\begin{bmatrix}\tilde{q}\\ \tilde{z}\end{bmatrix},\ \tilde{Y}=\begin{bmatrix}\hat{y}\\ \hat{y}_1\\ \hat{y}_2\end{bmatrix},\ \tilde{V}=\begin{bmatrix}\tilde{p}\\ \tilde{v}\end{bmatrix},\ \tilde{U}=\begin{bmatrix}\hat{u}_1\\ \hat{u}_2\end{bmatrix},$$

we can rewrite the above system as

$$\begin{bmatrix}\dot{\tilde{X}}\\ \tilde{Z}\\ \tilde{Y}\end{bmatrix}=\begin{bmatrix}A(\psi) & B_V(\psi) & B_U\\ C_Z(\psi) & D_{ZV}(\psi) & D_{ZU}\\ C_Y & D_{YV} & 0\end{bmatrix}\begin{bmatrix}\tilde{X}\\ \tilde{V}\\ \tilde{U}\end{bmatrix}, \quad (10)$$

where the matrices can be identified from Eq. (9). Suppose the varying parameter ψ belongs to a polytope Ψ of vertices $\psi_1, \psi_2, \ldots, \psi_n$, i.e. $\psi \in \Psi \triangleq \mathrm{Co}\{\psi_1, \psi_2, ..., \psi_n\}$. The state space matrices of Eq. (10) thus also belong to a polytope Ξ of matrices with vertices corresponding to images of the vertices $\psi_1, \psi_2, \ldots, \psi_n$. The LPVRC controller is determined by

$$\begin{bmatrix}A_K & B_K\\ C_K & D_K\end{bmatrix}=\sum_{i=1}^{n}\alpha_i\begin{bmatrix}A_{Ki} & B_{Ki}\\ C_{Ki} & D_{Ki}\end{bmatrix},$$

and (A_{Ki}, B_{Ki}, C_{Ki}, D_{Ki}) are controller matrices synthesized based on the state space matrices that correspond to the i^{th} vertex of the open-loop polytopic system, Eq. (10)[25].

IV. Experimental Results

For the experimental platform, the filter that upper bounds the output multiplicative modeling error is

$$W_2(s)=0.03\frac{s/16+1}{s/700+1}.$$

The selection of W_1 requires more considerations. It is pointed out by Wu et al. [26] that the LPV design will collapse to the case which is independent of the saturation indicator ϕ if the performance weighting does not depend on ϕ. It is also desirable to choose a parameter-dependent W_1 that does not destroy the polytopic nature of the LPV open-loop system. A feasible W_1 filter thus has the transfer function

$$W_1(s)=k+\frac{e\phi}{s+\omega_b\phi+b}.$$

The polytopic parameter variation set Ψ is selected as

$$\Psi=\{(\rho,\phi,\eta):\ 1\le\rho\le 10,\ 0.1\le\phi\le 1,\ \eta=\rho\phi\},$$

With the varying range of ϕ specified, the parameters of the weighting filter W_1 can be properly determined to reflect the different performance requirement for the unsaturated ($\phi = 1$)

and saturated ($\phi < 1$) system. The low-order attenuated repetitive controller can be expressed as

$$RC(s) = \frac{1}{s/(2\pi \times 200)+1} \prod_{\substack{\omega_n = 32,48,96 \\ \xi_n = 0.002,0.002,0.001}} \frac{s^2 + 2 \times 0.1 \times \omega_n s + \omega_n^2}{s^2 + 2 \times \xi_n \omega_n s + \omega_n^2},$$

where the periodic disturbances are at 32, 48 and 96 cycles/rev. A feasible LPV controller is determined from the above parameter settings.

The experiment was performed by activating the LPVRC controller and letting the photosensitive drum turn for 40 revolutions. During the operation, the nominal motor input voltage was changed at the 10th, 20th and 30th revolution, which shifted the nominal drum angular velocity. Figure 9 compares the frequency spectrum of the velocity signals within each 10-revolution position interval to that of the uncompensated system. We can see that the performance of the LPVRC controlled system is now insensitive to changes of the nominal drum angular velocity. Printed images from the uncompensated and compensated systems are shown in Fig. 10, in which banding rejection can be observed on the image from the compensated system. Another experiment with similar steps was conducted for the temporal-based repetitive control system. The results are demonstrated in Fig. 11. We can see that the temporal-based design is incapable of tackling changes of the nominal angular velocity.

V. Conclusion

In this paper, we proposed three different repetitive control based design for the reformulated nonlinear system in angular position (of photosensitive drum) domain. The immediately advantage is that the new repetitive control system is robust to those time-varying position-dependent periodic disturbances.

References

[1] R. Firth, D. Kessler, E. Muka, M. Noar, and J. Owens, "A continuous-tone laser color printer," *Journal of Imaging Technology*, vol. 14, no. 3, pp. 78-89, 1988.

[2] Y. Hotta, M. Goto, and T. Miyamoto, Image forming apparatus having relationship between driving gear pitch and scanning line pitch, *U.S. Patent* 5,917,529 (1999).

[3] P. L. Jeran, Gear train control system for reducing velocity induced image defects in printers and copiers, *U.S. Patent* 5,812,183 (1998).

[4] T. Kusuda, M. Ikeda, T. Ogiri, and T. Besshi, Transmission deviation caused by eccentricity in multi gear systems, in *PICS: Image Processing, Image Quality, Image Capture, Systems Conference*, Savannah, Georgia, pp. 119-124, 1999.

[5] R. J. Lawton and D. R. Marshall, Beam deflecting for resolution enhancement and banding reduction in a laser printer, *U.S. Patent* 5,920,336 (1999).

[6] W. E. Foote and R. G. Sevier, Laser printer with apparatus to reduce banding by servo adjustment of a scanned laser beam, *U.S. Patent* 5,760,817 (1998).

[7] K. Bannai, Image forming apparatus with anti-banding implementation, *U.S. Patent* 5,315,322 (1994).

[8] M. Ewe, J. Grice, G.T.-C. Chiu, J. Allebach, C.S. Chan, and W. Foote, "Banding reduction in electrophotographic processes using piezoelectric actuated laser beam deflection device," *Journal of Image Science and Technology,* Vol. 46, No. 5, pp. 433-442, September/October 2002.

[9] R. P. Loce and W. L. Lama, Printer compensated for vibration-generated scan line errors, *U.S. Patent* 4,884,083 (1989).

[10] D. W. Costanza, R. E. Jodoin, and R. P. Loce, Method and apparatus for compensating for raster position errors in output scanners, *U.S. Patent* 5,900,901 (1999).

[11] R. D. Morrison, System and method for modifying an output image signal to compensate for drum velocity variations in a laser printer, *U.S. Patent* 5,729,277 (1998).

[12] W. L. Lama, R. P. Loce, and J. A. Durbin, Image bar printer compensated for vibration-generated scan line errors, *U.S. Patent* 4,801,978 (1989).

[13] G.Y. Lin, J. Grice, J. Allebach, G.T.-C. Chiu, W. Bradburn, and J. Weaver, "Banding artifact reduction in electrophotographic printers by using pulse width modulation," *Journal of Image Science and Technology*, Vol. 46, No. 4, pp. 326-337, July/August 2002.

[14] C.-H. Li and J. Shu, Banding noise reduction for clustered-dot dither, *U.S. Patent* 5,875,287 (1999).

[15] J. Marsden, Reduction of banding in printed images, *U.S. Patent* 6,025,922 (2000).

[16] A. Silverstein and B. Chu, "Does error-diffusion halftone texture mask banding," in *NIP14: 2000 International Conference on Digital Printing Technologies*, Toronto, Canada, pp. 560-563, Oct. 1998.

[17] C.-L. Chen, G.T.-C. Chiu, and Jan P. Allebach, "Banding reduction in electrophotographic processes using human contrast sensitivity function shaped photoconductor velocity control," *Journal of Image Science and Technology*, Vol. 47, No. 3, pp. 209-223, May/June 2003.

[18] J. L. Mannos and D. J. Sakrison, "The effects of a visual fidelity criterion on the encoding of images", *IEEE Transactions on Information Theory*, vol. IT-20, no. 4, pp. 525-536, 1974.

[19] V. Virsu, P. Lehtio, and J. Rovamo, "Contrast sensitivity in normal and pathological vision," *Documenta Ophthalmologica Proceeding Series*, vol. 30, The Netherlands: Dr. W. Junk Publisher, 1981.

[20] P. Barten, "Evaluation of subjective image quality with the square-root integral method", *Journal of the Optical Society of America*, vol. 7, no. 10, pp. 2024-20331, 1990.

[21] T. Mitsa and J. R. Alford, "Single-channel versus multiple-channel visual models for the formulation of image quality measures in digital halftoning," in *NIP17: 10th International Congress on Advances in Non-Impact Printing Technologies*, New Orleans, Louisiana, pp. 14-16, 1994.

[22] D. R. Badcock, "The visual detection of spatial beats," *Human Information Processing: Measures, Mechanism and Models*, Elsevier Science Publishiers B.V., pp. 15-29, 1989.

[23] G. J. Burton, "Evidence for non-linear response processes in the human visual system from measurements on the thresholds of spatial beat frequencies," *Vision Research*, vol. 13, pp.1211-1225, 1973.

[24] A. D. Logvinenko, "Nonlinear analysis of spatial vision using first-and-second-order volterra transfer functions measurement," *Vision Research*, vol. 30, pp. 2031-2057, 1990.

[25] P. Gahinet, "Explicit controller formulas for LMI-based H∞ synthesis," *Automatica*, vol. 32, no. 7, pp.1007-1014, July 1996.

[26] F. Wu, K. M. Grigoriadis and A. Packard, "Anti-windup controller design using linear parameter-varying control methods," *International Journal of Control*, vol. 73, no. 12, pp. 1104-1114, 2000.

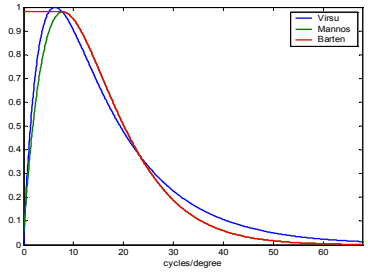

Figure 1: Human contrast sensitivity function (CSF)

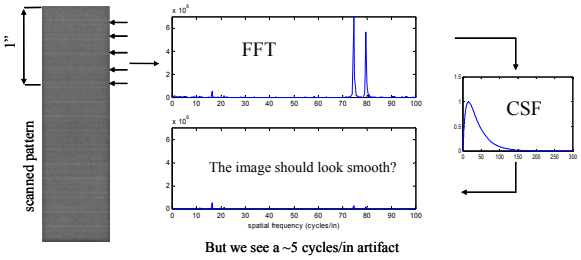

Figure 2: A simple example demonstrating frequency beat

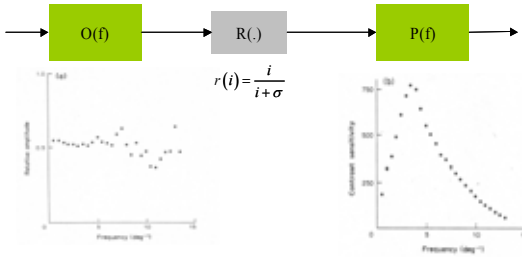

Figure 3: The cascade sandwich human visual model (Logvinenko)

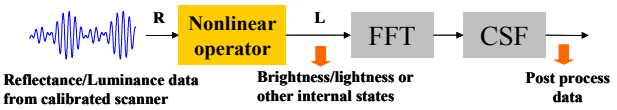

Figure 4: The proposed 3-stage human visual model.

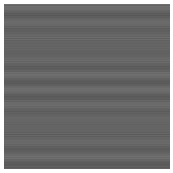

Figure 5: Mixed frequencies banding perception 4 frequencies.

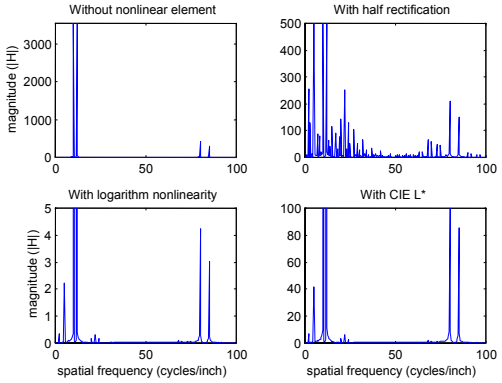

Figure 6: Results for simulation 3.

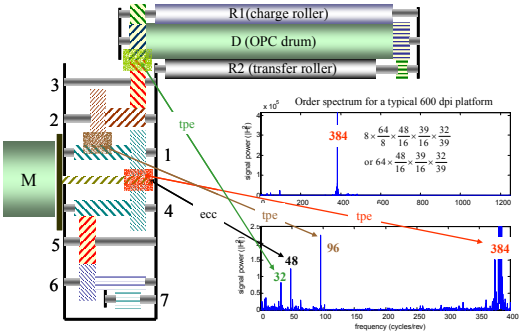

Figure 7: Motor/gear transmission subsystem of a laser printer.

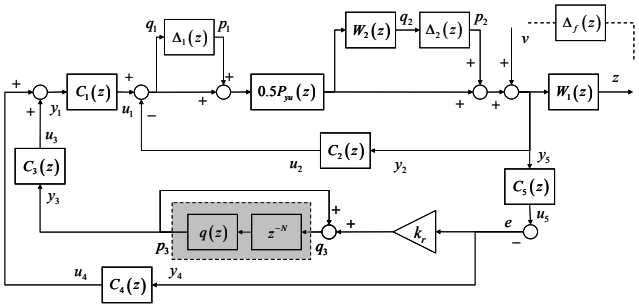

Figure 8: Control structure for the spatial-based repetitive control system.

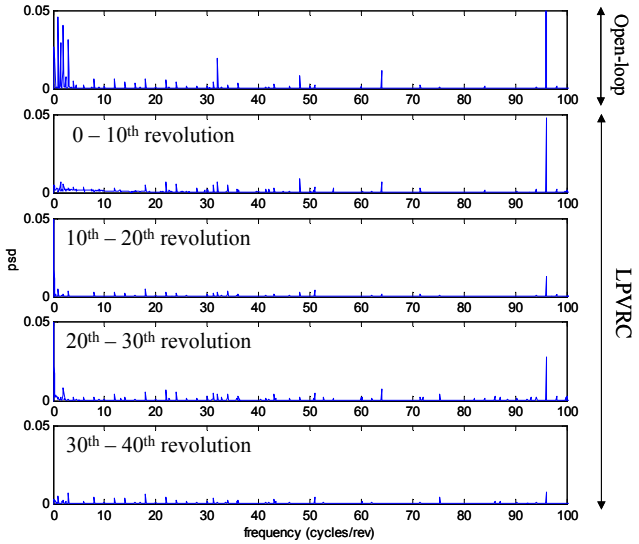

Figure 9: Frequency spectra of the velocity signals for the open-loop and closed-loop systems.

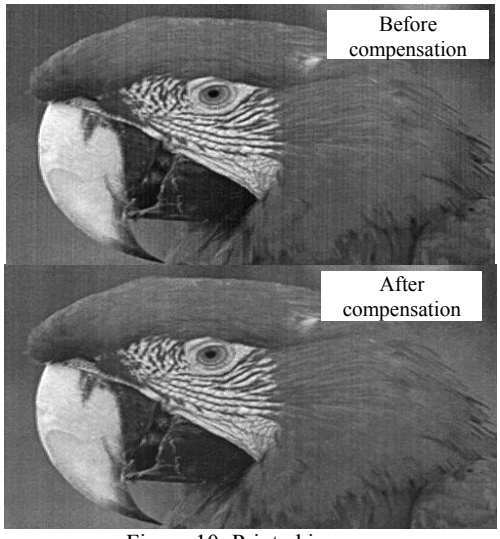

Figure 10: Printed images

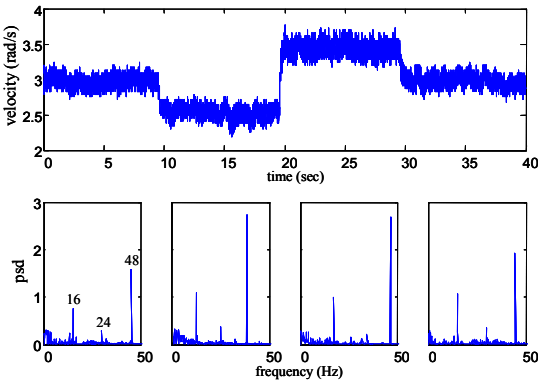

Figure 11: Time history and frequency spectra of the drum angular velocity signals from the temporal-based repetitive control system.